Alkali metal adducts of an iron(0) complex and their synergistic FLP-type activation of aliphatic C–X bonds

Tinnerman, Hendrik; Sung, Simon; Csókás, Dániel; Toh, Zhi Hao; Fraser, Craig; Young, Rowan

DOI:
10.1021/jacs.1c04815

Document Version
Peer reviewed version

Citation for published version (Harvard):
Tinnerman, H, Sung, S, Csókás, D, Toh, ZH, Fraser, C & Young, R 2021, 'Alkali metal adducts of an iron(0) complex and their synergistic FLP-type activation of aliphatic C–X bonds', *Journal of the American Chemical Society*, vol. 143, no. 28, pp. 10700-10708. https://doi.org/10.1021/jacs.1c04815

Alkali metal adducts of an iron(0) complex and their synergistic FLP-type activation of aliphatic C–X bonds

Hendrik Tinnermann‡, Simon Sung‡, Daniel Csokas, Toh Zhi Hao, Craig Fraser and Rowan D. Young*
Department of Chemistry, National University of Singapore, 3 Science Drive 3, Singapore 117543

ABSTRACT: *We report the formation and full characterization of weak adducts between Li^+ and Na^+ cations and a neutral iron(0) complex, $[Fe(CO)_3(PMe_3)_2]$ (**1**), supported by weakly coordinating $[BAr^F{}_{20}]$ anions, $[\mathbf{1}\bullet M][BAr^F{}_{20}]$ (M = Li, Na). The adducts are found to synergistically activate aliphatic C–X bonds (X = F, Cl, Br, I, OMs, OTf) leading to the formation of iron(II) organyl compounds of the type $[FeR(CO)_3(PMe_3)_2][BAr^F{}_{20}]$, of which several were isolated and fully characterized. Remarkably, $[\mathbf{1}\bullet M][BAr^F{}_{20}]$ is able to activate dichloromethane under mild conditions. Stoichiometric reactions with the resulting iron(II) organyl compounds show that this system can be utilized for homo-coupling and cross-coupling reactions and the formation of new C–E bonds (E = C, H, O, N, S). Further, we utilize $[\mathbf{1}\bullet M][BAr^F{}_{20}]$ as a catalyst in a simple hydrodehalogenation reaction under mild conditions to showcase its potential use in catalytic reactions. Finally, the mechanism of activation is probed using DFT and kinetic experiments that reveal that the alkali metal and iron(0) centre cooperate to cleave C–X via a mechanism closely related to intramolecular FLP activation.*

Introduction

The transfer of organyl groups from halides to metals is a key concept in organic synthesis and carbon-element bond formation. The transfer formally reduces the organyl group, transforming its nature from electrophilic to nucleophilic, and thus enabling the organyl moiety to be used in coupling chemistry. In most instances, the use of highly reducing metals, such as elemental lithium, magnesium or zinc, or the use of noble metals, such as rhodium or palladium, is required for such transformations to take place.[1] This requirement renders reactions either highly expensive (when using noble metals), or highly dangerous (when using highly reductive metals). To circumvent these limitations, there has been a recent push to utilize base metals for the activation and functionalization of organic halides.[2]

In this respect, electron rich ferrates have been successful for the activation of strong aliphatic-halide bonds allowing both reductive homo-coupling and cross-coupling reactions (Figure 1, A).[3] Such ferrates are typically supported by s-block cations, most commonly magnesium fragments, arising from precatalyst activation with Grignard reagents, or alkali metal counter-ions. In most of these systems counter-cations are thought to play little role in C–X bond activation and are often mechanistically ignored unless they are in the coordination sphere of iron.

In contrast, distinct synergistic effects for C–H activation/deprotonation have been observed for multiple ferrate/s-block metal combinations (Figure 1, B).[4] For example, Mulvey and Hevia have shown that combinations of ferrates with sodium counter ions are able to deprotonate arene hydrogen positions,[4a,b] Jouikov and Mongin used a putative lithium ferrate to deprotonate arenes *in situ* for subsequent electrophilic functionalization,[4c] and Knochel was able to metallate arene C–H positions through the combination of an iron(II) diamide, lithium chloride and magnesium chloride used *in situ*.[4d] To date, the ferrate components employed in both C–H and C–X activations are both highly basic and highly reducing, so must be handled under inert conditions. Activation of C–X or C–H bonds by non-ferrate iron systems is extremely rare.[4d]

Herein, we report on the use of robust and stable components in the synergistic activation of strong aliphatic C–X bonds by well-characterized cationic iron(0)-alkali metal adducts (Figure 1, C). We demonstrate their potential use in synthesis through stoichiometric homo-coupling reactions, stoichiometric cross-coupling reactions and catalytic hydrodehalolgenation reactions. Finally, we explore the mechanism of C–X activation through a combination of kinetic and DFT studies to elucidate the origin of the unexpected synergistic reactivity.

Results and Discussion

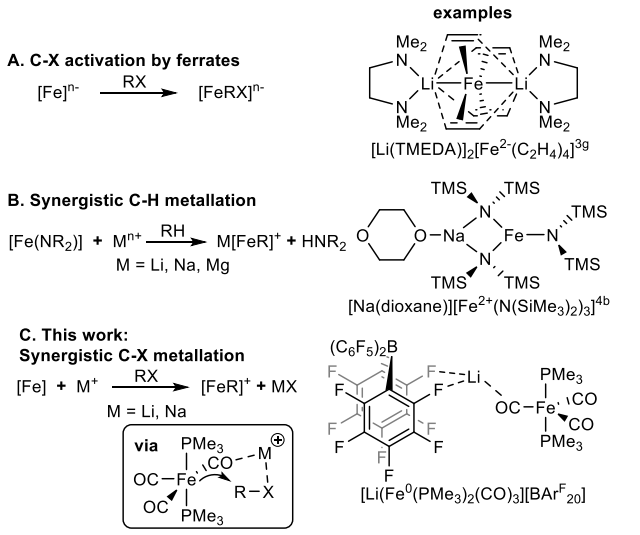

Figure 1. (**A**) Iron ferrates are known to activate sp^2 and sp^3 C–X bonds (X = Cl, Br, I).[3] (**B**) Iron amides and s-block metals are reported to synergistically deprotonate sp^2 C–H bonds.[4] (**C**) This work describes synergistic activation of sp^3 C–X bonds (X = F, Cl, Br, I, OMs, OTf) using an iron(0) complex with lithium and sodium salts.

Synthesis and characterization of adducts

Mixing of $[Fe(CO)_3(PMe_3)_2]$[5] (**1**) with non-solvated lithium or sodium salts of the weakly coordinating borate anion $[BAr^F{}_{20}]$ {$BAr^F{}_{20}$ = $B(C_6F_5)_4$}, results in the formation of adducts of the empirical form $[\mathbf{1}\bullet M][BAr^F{}_{20}]$ (M = Li, Na) (Scheme 1).

Crystals of $[\mathbf{1}\bullet M][BAr^F{}_{20}]$ (M = Li, Na), grown from layering fluorobenzene solutions of $[\mathbf{1}\bullet M][BAr^F{}_{20}]$ with *n*-hexane, reveal the solid state structures of the adducts (Figure 2). Compound **1** has been utilized as a Lewis base previously in frustrated Lewis pair (FLP) chemistry[6] and in metal-only Lewis pairs (MOLP) with both transition metals and main group metals,[7] allowing the direct formation of Lewis acid-iron bonds. In contrast, **1** binds hard Lewis acidic alkali metals through its carbonyl oxygen atoms (i.e. hard Lewis bases). Alkali metal adducts with iron carbonyl ligands are known, but only in ferrate complexes where a strong electrostatic interaction stabilizes the interaction.[8]

The molecular structure of $[\mathbf{1}\bullet Na][BAr^F{}_{20}]$ reveals three separate molecules of **1** bind sodium cations through their carbonyl oxygen atom (κ^1-O), with a further five coordination sites on the sodium cation being occupied by fluorine atoms of $[BAr^F{}_{20}]^-$ counter anions. Thus, a 2D-coordination polymer network is established via sodium-carbonyl coordination (Figure 2).

In the lithium adduct $[\mathbf{1}\bullet Li][BAr^F{}_{20}]$, only two carbonyls bind each lithium atom with the remaining three coordination sites occupied

Scheme 1. Formation of adducts [**1**•M][BAr^F_{20}] (M = Li, Na).

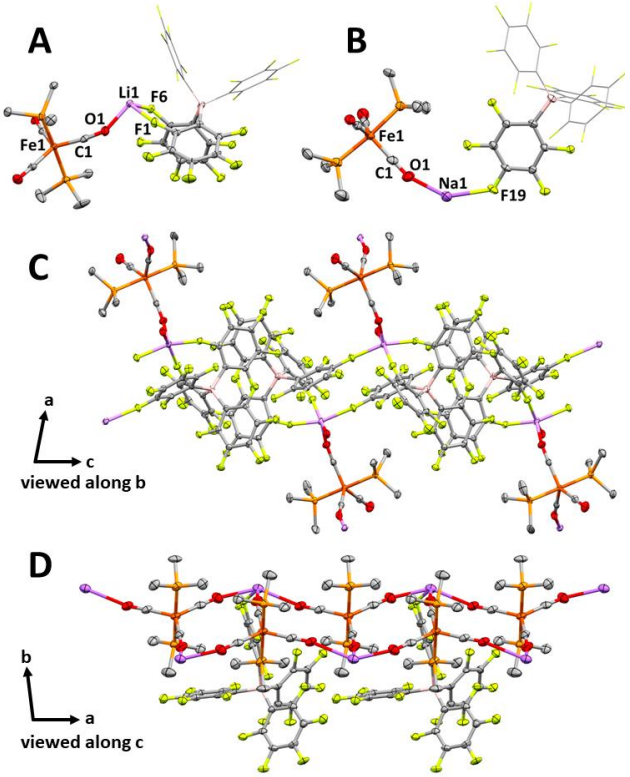

Figure 2. (**A**) Molecular structure of [**1**•Li][BAr^F_{20}], asymmetric unit. Selected bond distances (Å): Li1-O1, 1.952(6); Fe1-C1, 1.739(3). (**B**) Molecular structure of [**1**•Na][BAr^F_{20}], asymmetric unit. Selected distances (Å): Na1-O1, 2.331(5); Fe1-C1, 1.752(5). (**C**) Packing for [**1**•Li][BAr^F_{20}] viewed along b-axis. (**D**) Packing for [**1**•Na][BAr^F_{20}] viewed along c-axis. Hydrogen atoms omitted from all structures.

by fluorine atoms of the anions. Thus, a dimeric structure is established with respect to lithium/carbonyl coordination, although a coordination polymer structure is still present, but formed between the lithium cations and the [BAr^F_{20}]$^-$ anions.[9] The change in structure is likely resultant from a lower coordination number restriction arising from the smaller ionic radius of lithium (90 pm) as compared to sodium (116 pm).[10]

Structural differences between the lithium and sodium adducts in the solid state are supported by infrared spectroscopy. A nujol mull FTIR spectrum of [**1**•Li][BAr^F_{20}] displays two carbonyl bands at 1834 cm^{-1} and 1819 cm^{-1} (*c.f.* compound **1** ν_{CO} = 1879 cm^{-1}), while that of [**1**•Na][BAr^F_{20}] shows two bands at 1871 cm^{-1} and 1849 cm^{-1}, indicating a weaker Fe–CO···M interaction. This is reflected in the molecular structures of [**1**•M][BAr^F_{20}], where the comparative Fe–C**O**···**Na** distances {ranging from 2.331(5) to 2.732(5) Å} and Fe–C**O**···**Li** distances {ranging from 1.952(6) to 2.031(5) Å} are well beyond the difference in ionic radii between lithium and sodium (26 pm).[10]

Solution studies of [**1**•M][BAr^F_{20}] (M = Li, Na) indicate that a degree of association is maintained between the alkali metals and **1** (Table 1). ESI-Mass spectrometry of solutions of [**1**•M][BAr^F_{20}] reveals signals at 591.0312 *m/z* and 607.0123 *m/z* corresponding to the adducts [$\mathbf{1_2}$•M]$^+$ (M = Li, Na) respectively. ^{31}P NMR spectroscopy of [**1**•M][BAr^F_{20}] (M = Li, Na) shows a very slight upfield shift (<1 ppm) of the PMe_3 signals from **1** (δ_P 38.4), as well as

Table 1. Possible speciation of [**1**•M][BAr^F_{20}] in solution.

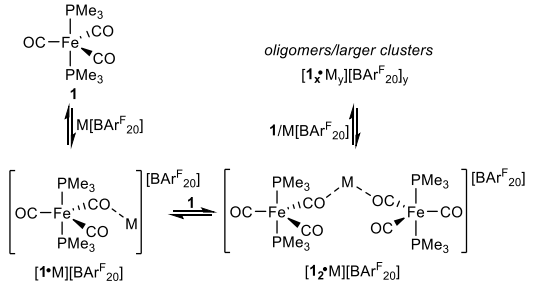

species	diffusion rate (10^{-10} m^2 s^{-1})	species observed by ESI-TOF-MS
1	11.20 (**1**)	-
1 + Li[BAr^F_{20}]	7.37 (**1**)	[**1**•Li]$^+$, [$\mathbf{1_2}$•Li]$^+$
1 + Na[BAr^F_{20}]	8.93 (**1**)	[**1**•Na]$^+$, [$\mathbf{1_2}$•Na]$^+$
1 + K[BAr^F_{20}]	10.93 (**1**)	[**1**•K]$^+$
1 + Na[BAr^F_{24}]	8.04 (**1**), 5.74 (BAr^F_{24})	[**1**•Na]$^+$, [$\mathbf{1_2}$•Na]$^+$
Na[BAr^F_{24}]	6.47 (BAr^F_{24})	-

broadening of the signals, indicating that dynamic alkali metal exchange likely occurs. Indeed, an equilibrium between coordinated and 'free' alkali metal ions was established by the addition of 0.5, 1.0 and 2.0 equivalents of Na[BAr^F_{20}] to **1**, resulting in a shift of the ^{31}P resonance from δ_P 38.3 to 38.0 to 37.8.

^{1}H DOSY NMR experiments also establish that **1** and M[BAr^F_{20}] (M = Li, Na) are strongly associated in solution. For example, the ^{1}H NMR signal of PMe_3 in a sample of **1** in 1,2-DFB corresponds to a diffusion coefficient of 11.20 x10^{-10} m^2 s^{-1}, while addition of 1 equiv. of M[BAr^F_{20}] to the sample reduces the signal's diffusion coefficient to 7.37 x10^{-10} m^2 s^{-1} (Li) or 8.93 x10^{-10} m^2 s^{-1} (Na). Addition of K[BAr^F_{20}] provides only a minor reduction in diffusion coefficient to 10.93 x10^{-10} m^2 s^{-1}, consistent with our inability to isolate and characterize [**1**•K][BAr^F_{20}] in the solid state, although mass spectrometric data also indicated a concentration of [**1**•K][BAr^F_{20}] in solution (Table 1). Given the relative size of the alkali metals, the DOSY NMR data suggest that adduct formation is favored with the preference Li>Na>K resulting in the observed average diffusion coefficients.

Lithium and sodium salts of the related borate anion [BAr^F_{24}]$^-$ {BAr^F_{24} = tetrakis(3,5-bis(trifluoromethyl)phenyl)borate} were found to form similar adducts with correlating spectroscopic and spectrometric data. DOSY ^{1}H NMR spectra of Na[BAr^F_{24}] added to **1** also show a decrease in the diffusion coefficient to 8.04 x10^{-10} m^2 s^{-1}. Further, the diffusion coefficients of the [BAr^F_{24}]$^-$ anion aryl protons are reduced from a sample of pure Na[BAr^F_{24}] in 1,2-DFB (see Table 1), suggesting that the anion is also interacting with **1**. Indeed, calculations indicated complete dissociation of the [BAr^F_{20}]$^-$ anion from [**1**•Na]$^+$ to be endogonic by 8.2 kcal mol^{-1} and that the alkali metal is likely supported by the anion in solution.

We also attempted to establish the relative thermodynamic stability of possible adducts in solution using DFT. However, these calculations showed that many permutations of [$\mathbf{1_x}$•Na_y][BAr^F_{20}]$_y$ (and their solvates) are possible within computational error (i.e. ± 2 kcal mol^{-1}). Although these spectroscopic, spectrometric and computational data cannot explicitly establish the precise speciation of [**1**•M][BAr^F_{20}] in solution, they do imply that significant interaction between **1** and the alkali metal is persistent, and that the interaction follows the order of Li>Na>K.

C–X activation chemistry

Compound **1** and the salts M[BAr^F_{20}] (M = Li, Na, K) are separately stable in halogenated alkane solvents and in the presence of alkyl halides. However, the adducts [**1**•M][BAr^F_{20}] were found to activate a variety of aliphatic C–X bonds under surprisingly mild reac-

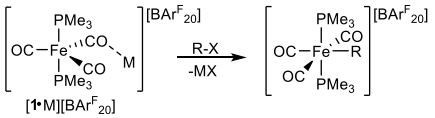

Table 2. Qualitative activation of C–X substrates. Selected reactions from Table S2, see SI.

entry	substrate	salt	time/temp	conversion
1	BnCl	Li[BAr$^{F}_{20}$]	5 h/25 °C	100%
2	BnCl	Na[BAr$^{F}_{20}$]	72 h/25 °C	65%
3	BnCl	Na[BAr$^{F}_{20}$]	4 h/80 °C	100%
4	BnCl	K[BAr$^{F}_{20}$]	24 h/25 °C	<5%
5	BnCl	none	16 h/80 °C	<5%
6	BnBr	Li[BAr$^{F}_{20}$]	5 h/25 °C	100%
7	*p*-TolCF$_2$H	Li[BAr$^{F}_{20}$]	1 h/25 °C	100%
8	BnOMs	Na[BAr$^{F}_{20}$]	1 h/25 °C	100%
9	MeOTf	Na[BAr$^{F}_{20}$]	1 h/25 °C	100%
10	*t*-BuCl	Li[BAr$^{F}_{20}$]	1 h/25 °C	100%
11	*n*-OctF	Li[BAr$^{F}_{20}$]	24 h/25 °C	24%
12	*neo*-PentCl	Li[BAr$^{F}_{20}$]	16 h/25 °C	100%
13	CH_2Cl_2	Li[BAr$^{F}_{20}$]	3 h/60 °C	100%
14	CH_2Br_2	Li[BAr$^{F}_{20}$]	16 h/25 °C	100%
15	PhCl	Li[BAr$^{F}_{20}$]	24 h/80 °C	<5%

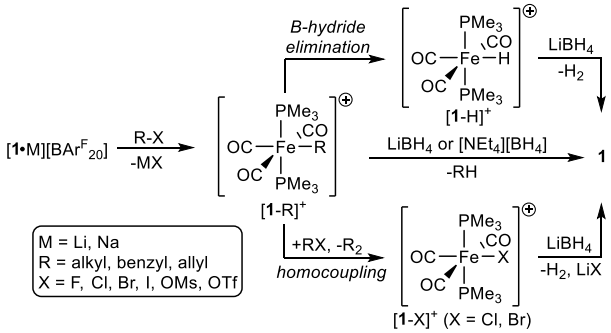

Scheme 2. Reactivity of [**1**•M][BAr$^{F}_{20}$] (M = Li, Na) with alkyl, benzyl and allyl halides. In the case of alkyl halides with an α-hydrogen, β-hydride elimination led to [**1**-H]$^+$. In the case of benzyl and allyl chlorides and bromides, homocoupling lead to [**1**-X]$^+$ (X = Cl, Br). Iron organyl, hydride and halide complexes could be reduced to the starting material (**1**) with borohydride reductant. Anions omitted for clarity.

tion conditions. For example, benzyl chloride was completely consumed by [**1**•Li][BAr$^{F}_{20}$] at room temperature in less than 5 hours to generate [**1**-Bn][BAr$^{F}_{20}$] (Table 2, entry 1). Similarly, [**1**•M][BAr$^{F}_{20}$] (M = Na, K) were found to activate benzyl chloride, albeit more slowly than [**1**•Li][BAr$^{F}_{20}$] (entries 2-4, Table 2 and Figure S10, see SI). However, in the absence of any alkali salt, compound **1** was found to be completely unreactive with benzyl chloride, even with prolonged heating (entry 5, Table 2).

Qualitative reactions between [**1**•M][BAr$^{F}_{20}$] (M = Li, Na, K) and a number of organyl halides and pseudohalides were undertaken to assess their reactivity patterns (Table 2 and Table S2, see SI). In summary, the adducts [**1**•M][BAr$^{F}_{20}$] efficiently activated primary, secondary and tertiary aliphatic halides, and allylic and benzylic halides. Alkyl fluorides, chlorides, bromides, iodides, mesylates and triflates were activated by [**1**•M][BAr$^{F}_{20}$] (M = Li, Na) but aryl halides possessing an sp^2 C–X bond did not react, even at elevated temperatures.

Astoundingly, [**1**•M][BAr$^{F}_{20}$] (M = Li, Na) was found to react with dichloromethane (DCM) at room temperature to generate [**1**-CH$_2$Cl][BAr$^{F}_{20}$] over a matter of days. At elevated temperatures, full conversion could be achieved in 3 hours (Table 2, entry 13). This is noteworthy, as although the activation of DCM by noble metals is well established,[11] C–Cl cleavage of DCM by iron (or other first row transition metals) is extremely rare and exemplifies the enhanced synergetic reactivity of [**1**•M][BAr$^{F}_{20}$].[12]

In substrates with α-hydrogen atoms relative to the C–X bond, β-hydride elimination of the iron alkyl activation product resulted in

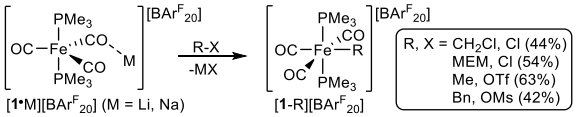

Scheme 3. Synthesis of isolated compounds [**1**-R][BAr$^{F}_{20}$] (R = CH$_2$Cl, Me, MEM, Bn) from reaction between [**1**•M][BAr$^{F}_{20}$] (M = Li, Na) with DCM, MEMCl, MeOTf and BnOMs respectively.

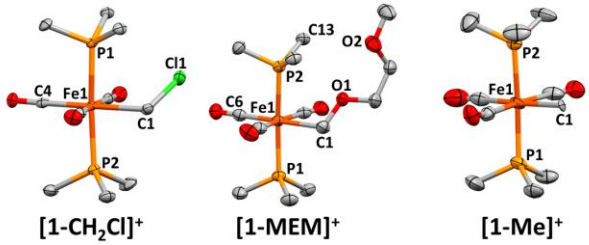

Figure 3. Molecular structures of [**1**-CH$_2$Cl][BAr$^{F}_{20}$], [**1**-MEM][BAr$^{F}_{20}$] and [**1**-Me][BAr$^{F}_{20}$]. Hydrogen atoms and anion omitted, thermal ellipsoids shown at 50%. Selected bond distances (Å) and angles (°): for [**1**-CH$_2$Cl]$^+$, Fe1-P1, 2.278(1); Fe1-P2, 2.270(1); Fe1-C1, 2.081(3); C1-Fe1-C4, 178.5(1); P1-Fe1-P2, 175.6(1); for [**1**-MEM]$^+$, Fe1-P1, 2.266(1); Fe1-P2, 2.284(1); Fe1-C1, 2.078(4); C1-Fe1-C6, 176.3(2); P1-Fe1-P2 173.6(1); for [**1**-Me]$^+$, Fe1-P1, 2.263(1); Fe1-P2, 2.264(1); Fe1-C1, 2.06(2); P1-Fe1-P2 177.3(1).

generation of [**1**-H][BAr$^{F}_{20}$][6] and concomitant formation of alkene by-product (Scheme 2). Further, in the presence of excess benzylic halides homocoupling was observed to generate the corresponding bibenzyl products and iron halide by-products [**1**-X][BAr$^{F}_{20}$][13] (X = Cl, Br). These complexes were also synthesized independently to verify their observed data.

As stated above, lithium and sodium salts of the related borate anion [BAr$^{F}_{24}$]$^-$ provided similar adduct formation and activation chemistry to M[BAr$^{F}_{20}$] (M = Li, Na) salts. However, no evidence was observed for adducts between **1** and group 1 metal salts containing less weakly coordinating counteranions ([BF$_4$]$^-$, [PF$_6$]$^-$, [SbF$_6$]$^-$, [BPh$_4$]$^-$, [OTf]$^-$, [ClO$_4$]$^-$). Nonetheless, combinations of **1** with a variety of alkali metal salts were tested for the activation of benzyl chloride, with only minor activation products observed (see SI, Tables S2 and S3).

Donating solvents were also found to obstruct activation. For instance the use of neat Et$_2$O, THF, 1,2-DME or MeOH as solvents hinders the activation of benzyl chloride by [**1**•M][BAr$^{F}_{20}$] (M = Li, Na) (see SI, Tables S2 and S3). This effect was illustrated by the addition of 10 equiv. of pyridine to the activation reaction of BnBr by [**1**•Na][BAr$^{F}_{20}$] that quenched the reaction. While the addition of 10 equiv. of Et$_2$O only slightly reduced the reaction rate (see SI, Figure S11). In general, polar arene solvents (PhCl, PhF, 1,2-C$_6$H$_4$F$_2$) provided the best solubility and least interference with the synergistic activation process.

Compounds [**1**-R][BAr$^{F}_{20}$] (R = Bn, CH$_2$Cl, Me, MEM {MEM = CH$_2$O(CH$_2$)$_2$OMe}) were isolated and fully characterized to confirm the identity of a number of activation products (Scheme 3). For example, compound [**1**-CH$_2$Cl][BAr$^{F}_{20}$] could be isolated in 44% yield and is identified by a triplet signal at 3.36 ppm ($^3J_{PH}$ = 8.3 Hz) in the ^{1}H NMR spectrum arising from the chloromethyl ligand and a single ^{31}P NMR resonance at δ 12.9. The chloromethyl ligand could also be identified in the ^{13}C NMR spectrum of [**1**-CH$_2$Cl][BAr$^{F}_{20}$] as a triplet signal at 32.4 ppm (t, $^2J_{PC}$ = 14.1 Hz). FTIR spectroscopy reveals three carbonyl stretching bands at 1990, 2043 and 2095 cm^{-1}, indicative of an iron(II) centre. The molecular structure of [**1**-CH$_2$Cl][BAr$^{F}_{20}$] displays octahedral geometry and confirms the activation of DCM, with a chloromethyl ligand observed to occupy an equatorial position with the three carbonyl ligands, while the phosphine ligands remain in the axial positions (Figure 3).

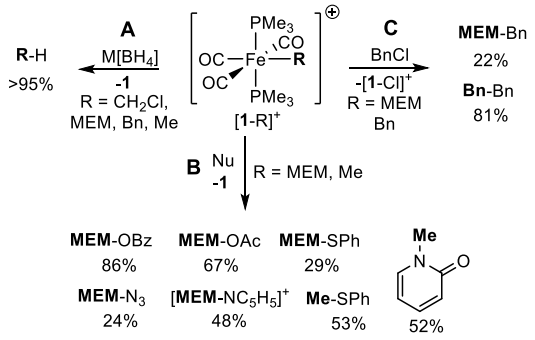

Scheme 4. (**A**) Reaction of [**1**-R]$^+$ with M[BH_4] (M = Li, NEt_4). (**B**) Reactions between [**1**-R]$^+$ and nucleophiles. (**C**) Reaction between [**1**-R]$^+$ and benzyl chloride. Anions omitted for clarity. See SI for details.

The characterization data of compounds [**1**-R][$BAr^F{}_{20}$] {R = Bn, Me, MEM} are unremarkable and similar to those of [**1**-

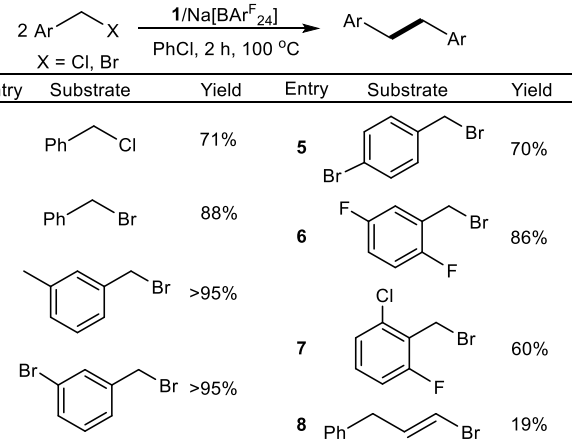

Figure 4. Homocoupling of benzyl halides using stoichiometric quantities of *in situ* generated [**1**•Na][$BAr^F{}_{24}$]. General conditions: **1** (0.04 mmol), Na[$BAr^F{}_{24}$] (0.04 mmol), substrate (0.08 mmol), solvent (0.5 mL). Yields determined by ^{1}H NMR spectroscopy.

CH_2Cl][$BAr^F{}_{20}$], but confirm the installation of MEM, Me and Bn alkyl groups onto the iron centre in their respective compounds.

Functionalization chemistry and potential use in catalysis

To demonstrate the synthetic potential of this system, some simple stoichiometric and catalytic organic transformations were explored. Complexes [**1**-R][$BAr^F{}_{20}$], [**1**-H][$BAr^F{}_{20}$] and [**1**-X][$BAr^F{}_{20}$] could be reduced with soluble forms of borohydride {*viz*. [NEt_4][BH_4] or Li[BH_4]} to cleanly reform **1** with concomitant formation of the corresponding [$BAr^F{}_{20}$]$^-$ salts (Scheme 2). In the cases of [**1**-R][$BAr^F{}_{20}$], the alkyl ligand was liberated as the corresponding alkane in near quantitative yield (Scheme 4, A). Compounds [**1**-R][$BAr^F{}_{20}$] (R = Bn, Me, MEM) was also probed with various nucleophiles to generate cross-coupled products (Scheme 4, B). Concurrent with the reaction with these nucleophiles, compound **1** was generated as the major by-product. Compounds [**1**-R][$BAr^F{}_{20}$] (R = MEM, Bn) also facilitated formal reductive coupling with electrophiles, for example reaction of [**1**-MEM][$BAr^F{}_{20}$] with BnCl generated the cross coupled product MEM-Bn in 22% yield along with [**1**-Cl][$BAr^F{}_{20}$] (Scheme 4, C), while [**1**-Bn][$BAr^F{}_4$] generated bibenzyl in 81% yield under the same conditions.

The high yield of bibenzyl from reaction of [**1**-Bn][$BAr^F{}_4$] with BnCl led us to explore stoichiometric reductive homocouplings using [**1**•Na][$BAr^F{}_{24}$] with organyl halides (Figure 4).[3c,14] Under relatively mild conditions, most benzyl halide substrates gave good to

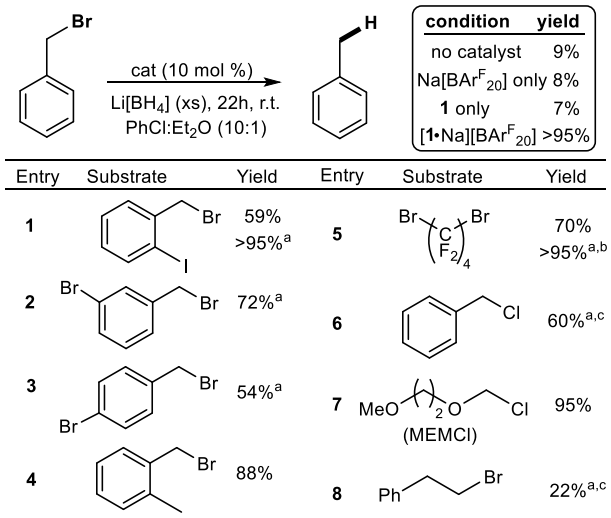

Figure 5. Catalytic reduction of aliphatic halides using 10 mol % of [**1**•Na][$BAr^F{}_{20}$]. General conditions: **1** (0.01 mmol), Na[$BAr^F{}_{20}$] (0.01 mmol), substrate (0.1 mmol), PhCl (0.5 mL), Et_2O (0.05 mL), Li[BH_4] (0.5 mmol). Yields determined by ^{1}H NMR spectroscopy. [a] Reaction performed at 60 °C. [b] Both bromides reduced. [c] $CF_3CH(OH)CF_3$ used in place of Et_2O.

excellent yields of their corresponding bibenzyl products (Figure 4, entries 1-7). Allylic bromides also produced homocoupled products in low yields (Figure 4, entry 8), however, for substrates containing α-hydrogen atoms (relative to the halide position), fast β-hydride elimination generated the iron hydride [**1**-H][$BAr^F{}_{24}$], and prevented the homocoupling reaction.

Finally, given that the elements of C–X activation and reduction of activation compounds [**1**-R][$BAr^F{}_{20}$] to reform **1** have been demonstrated above, we developed a simple catalytic reaction allowing for hydrodehalogenation of alkyl halides (Figure 5).[15] In the absence of [**1**•M][$BAr^F{}_{20}$] (M = Li, Na), Li[BH_4] acts as a poor reductant for aliphatic halides, as evidenced by the direct reaction of benzyl bromide and Li[BH_4] giving less than 10% yield of toluene after 22 hours at room temperature. In contrast, the addition of catalytic amounts of [**1**•Na][$BAr^F{}_{20}$] reduces benzyl bromide quantitatively under the same conditions (Figure 5). In these reactions, a small amount of Et_2O was added to assist dissolution of Li[BH_4], however, it was found that higher concentrations of Et_2O disrupted synergistic cooperation between **1** and Na^+, and hindered C–X activation.

A brief substrate scope assay showed that a range of alkyl halides (benzylic and non-benzylic) could be catalytically reduced in moderate to good yields, with aliphatic chlorides proving more difficult than aliphatic bromides as would be expected (Figure 5). More importantly, this reaction exemplifies the synthetic potential of this mild synergistic system, and we are currently developing other catalytic reactions using [**1**•M][$BAr^F{}_{20}$] (M = Li, Na) focused on C–C and C–E (E = N, O, S) coupling reactions.

Mechanistic insight into C–X activation

We postulated that coordination of the alkali metal (Li or Na) to the alkyl halide position likely reduces the barrier for S_N2 attack by **1**, in a mechanism reminiscent of FLP activation of alkyl fluorides.[16] A series of kinetic experiments were performed to support our hypothesis. Initial rates experiments between BnBr, **1** and Na[$BAr^F{}_{20}$] reveal that the reaction is first order with respect to **1**, BnBr and Na[$BAr^F{}_{20}$] (Figures S3-8, see SI). These data suggest an S_N2 type activation involving [**1**•Na][$BAr^F{}_{20}$] rather than larger dimetallic species such as [**1**$_2$•Na][$BAr^F{}_{20}$], which would be expected to follow a second order rate in **1**.

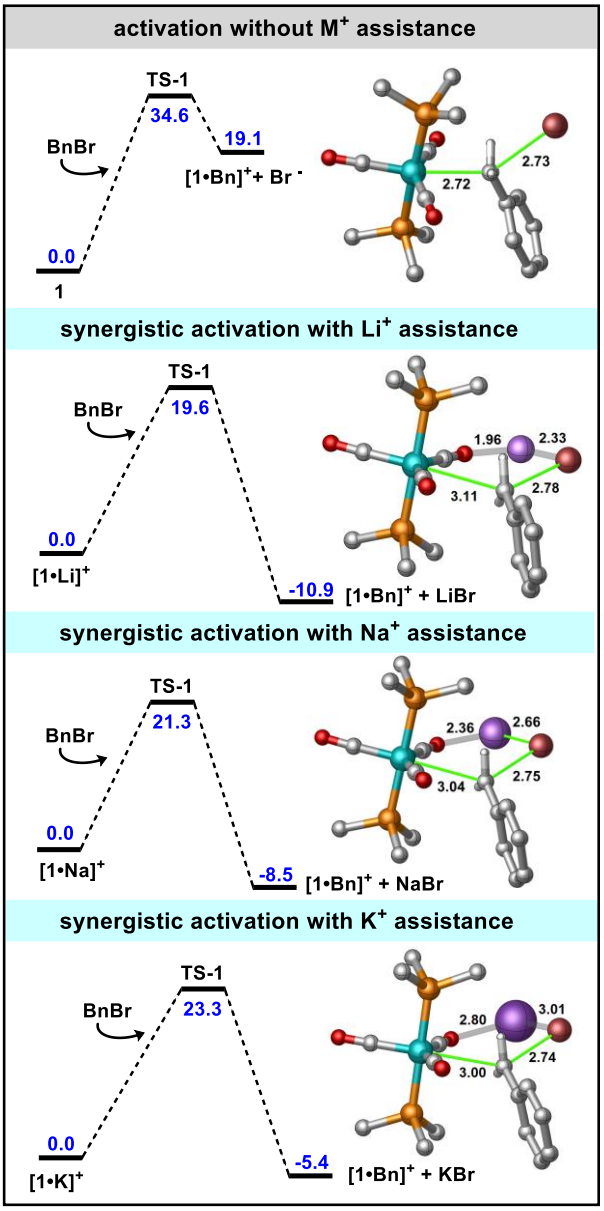

Figure 6. Calculated reaction profile for the nucleophilic activation of BnBr by **1** with and without M^+ (M = Li, Na, K) assistance (wB97X-D/Def2TZVPP//wB97X-D/Def2SVP(SMD), kcal mol^{-1}). Calculated structures for TS-1 included as insets with bond distances given in Å.

Evidence for a Lewis acid assisted S_N2 mechanism was also obtained from a Hammett plot from the activation of various benzyl bromides (Figure S13). The Hammett plot provided a ρ-value of -2.2, indicative of modest electron flow away from the benzyl aromatic ring in the transition state. This is consistent with coordination of a Lewis acid to the benzyl bromide position in the transition state. In contrast, S_N1 type activations have ρ-values below -4, and radical benzyl addition to iron is reported to have a positive ρ-value.[17]

To further rule out the possibility of a radical pathway for the activation of benzyl halides, 10 equiv. of the radical scavenger 1,4-methylcyclohexadiene (1,4-CHD) was added to a reaction between BnBr and [**1**•Na][BAr^F_{20}]. The presence of 1,4-CHD made no difference to the rate of reaction or yield of [**1**-Bn]$^+$ (see SI, Table S2).[18] However, 1,4-methylcyclohexadiene was found to significantly reduce the yield of the reductive homocoupling reaction for BnBr (Table S3, see SI), implying that reaction of BnBr with [**1**-Bn]$^+$ does proceed via a radical mechanism.[3c]

The activation of C–X bonds by [**1**•M][BAr^F_{20}] was also interrogated computationally using DFT. As a model system, we focused on the activation of benzyl bromide to generate [**1**-Bn]$^+$. Although a number of mechanistic possibilities were considered (see SI, DFT studies, alternative pathways), we focused our attention on the reaction pathway involving S_N2 attack of BnBr by **1** in the presence and absence of alkali metal cations. The reaction profile was calculated with a number of functionals (*viz.* ωB97X-D, M06, M06L), and anion and solvation effects were also modelled (see SI, Figures S71-77). However, similar trends and activation barriers were consistently observed regardless of the functional employed.

Figure 6 exemplifies the observed reaction trend in the presence and absence of M^+ (M = Li, Na, K). In the absence of any alkali metal cation, the barrier to C–Br activation is kinetically inaccessible (>30 kcal mol^{-1}). However, the inclusion of Li, Na or K lowers the transition state barrier by 15.0 to 11.3 kcal mol^{-1} (relative to the ground state) with the activation barriers following the order Li<Na<K. This result was corroborated with experimental kinetic data that showed the activation of BnBr by [**1**•M][BAr^F_{20}] (M = Li, Na, K) followed the reaction rate order of Li>>Na>K (see SI, Figure S10).

The inclusion of the alkali metal transforms the reaction from endogonic to exogonic, providing thermodynamic drive for the formation of [**1**-Bn]$^+$. In addition, precipitation of metal halide salt from activation reactions aided formation of [**1**-Bn]$^+$, which is not captured with these computational results.

Notably, calculations predict that C–X activation by [**1**•M]$^+$ proceeds via an intramolecular FLP type transition state (TS-1, with the alkali metal supported by the carbonyl ligand during the activation step. This transition state is reminiscent of calculated structures involved in the intramolecular FLP type activation of H_2 by $(LiP^tBu_2)_n$,[19] and is distinct from reactions employing Collman's Reagent that are hindered by coordinated alkali metals.[3q]

The computed free energy data lend strong support to our mechanistic proposal that the reaction proceeds via an 'assisted' S_N2 mechanism wherein the M^+ alkali metal cation contributes to a pronounced reduction in activation barrier height, mimicking FLP type reactivity. Such a mechanism is a distinct departure from oxidative addition, nucleophilic and radical processes more commonly observed in first row transition metal alkyl halide activation.[3,20]

Summary

In summary, we have found that in the absence of any competing base, lithium and sodium cations form weak adducts with **1** {[**1**•M][BAr^F_{20}] (M = Li, Na)} bonding through the carbonyl oxygen atoms. The cations in [**1**•M][BAr^F_{20}] (M = Li, Na) are further supported by their weakly coordinating [BAr^F_{20}] counter anions in the solid state, forming a coordination polymer, but likely exist as a dynamic mixture of adducts in solution. The introduction of aliphatic halides to solutions of [**1**•M][BAr^F_{20}] (M = Li, Na) results in C–X activation (X = F, Cl, Br, I, OMs, OTf), and the formation of iron(II) organyls of the type [**1**-R][BAr^F_{20}]. The remarkable enhanced reactivity afforded to **1** by the coordinated alkali metals means that their role in other iron mediated C–X activation reactions should not be overlooked.

It is shown that installed organyl ligands on compounds [**1**-R][BAr^F_{20}] (R = CH_2Cl, Me, Bn, MEM) can undergo subsequent functionalization through cross-coupling and homocoupling reactions, resulting in the formation of new C–H, C–C, C–O, C–S and C–N bonds. The catalytic potential of [**1**•M][BAr^F_{20}] (M = Li, Na) is demonstrated through hydrodehalogenation reactions with Li[BH_4]. The expansion of potentially useful functionalization reactions using this synergistic system is still under investigation.

Finally, the mechanism of our reaction was revealed through DFT analysis and kinetic experiments. These predict an intramolecular

bimetallic cooperative FLP type pathway, which represents a clear departure from conventional metal mediated C–X activations.

ASSOCIATED CONTENT

The Supporting Information, including experimental details and crystallographic data, is available free of charge on the ACS Publications website.

AUTHOR INFORMATION

Corresponding Author

*rowan.young@nus.edu.sg

‡ These authors contributed equally

ACKNOWLEDGMENT

We thank the Singapore Agency for Science, Technology and Research (A*STAR grant No. A1983c0033) for financial support.

REFERENCES

(1) Knochel, P.; Molander, G. A. Comprehensive Organic Synthesis, 2nd ed.; Elsevier: Amsterdam, The Netherlands, 2014.

(2) (a) Bauer, I.; Knölker, H. -J. Iron Catalysis in Organic Synthesis. *Chem. Rev.* **2015**, *115*, 3170; (b) Chirik, P.; Morris, R. Iron- and Cobalt-Catalyzed Alkene Hydrogenation: Catalysis with Both Redox-Active and Strong Field Ligands. *Acc. Chem. Res.* **2015**, *48*, 2495; (c) Bolm, C, A new iron age. *Nat., Chem*. **2009**, *1*, 420.

(3) (a) Makoa, T. L.; Byers, J. A. Recent advances in iron-catalysed cross coupling reactions and their mechanistic underpinning. *Inorg. Chem. Front.*, **2016**, *3*, 766; (b) Sherry, B. D.; Fürstner, A. The Promise and Challenge of Iron-Catalyzed Cross Coupling. *Acc. Chem. Res*., **2008**, *41*, 1500; (c) Hill, D. H.; Parvez, M. A.; Sen, A. Mechanistic Aspects of the Reaction of Anionic Iron(0)-Olefin Complexes with Organic Halides. Detection and Characterization of Paramagnetic Organometallic Intermediates. *J. Am. Chem. Soc*., **1994**, *116*, 2889; (d) Jonas, K.; Schieferstein, L.; Krüger, C.; Tsay, Y. -H. Tetrakis(ethylene)irondilithium and Bis(η^4-1,5-cyclooctadiene)irondilithium. *Angew. Chem., Int. Ed.*, **1979**, *18*, 550; (e) Bazhenova, T. A.; Kachapina, L. M.; Shilov, A. E. Mono- and binuclear σ-aryl iron-lithium hydrides; synthesis and molecular structure. *J. Organomet. Chem*., **1992**, *428*, 107; (f) Alonso, P. J.; Arauzo, A. B.; Fornies, J.; Garcia-Monforte, M. A.; Martin, A.; Martinez, J. I.; Menjon, B.; Rillo, C.; Saiz-Garitaonandia, J. J. A square-planar organoiron(III) compound with a spin-admixed state. *Angew. Chem., Int. Ed.*, **2006**, *45*, 6707; (g) Fürstner, A.; Martin, R.; Krause, H.; Seidel, G.; Goddard, G.; Lehmann, C. W. Preparation, Structure, and Reactivity of Nonstabilized Organoiron Compounds. Implications for Iron-Catalyzed Cross Coupling Reactions. *J. Am. Chem. Soc.* **2008**, *130*, 8773; (h) Sun, C. -L.; Krause, H.; Fürstner, A. A Practical Procedure for Iron-Catalyzed Cross-Coupling Reactions of Sterically Hindered Aryl-Grignard Reagents with Primary Alkyl Halides. *Adv. Synth. Catal*. **2014**, *356*, 1281; (i) Bedford, R. B.; Brenner, P. B.; Carter, E.; Cogswell, P. M.; Haddow, M. F.; Harvey, J. N.; Murphy, D. M.; Nunn, J.; Woddall, C. H. TMEDA in iron-catalyzed Kumada coupling: amine adduct versus homoleptic "ate" complex formation. *Angew. Chem., Int. Ed*. **2014**, *53*, 1804; (j) Al-Afyouni, M. H.; Fillman, K. L.; Brennessel, W. W.; Neidig, M. L. Isolation and Characterization of a Tetramethyliron(III) Ferrate: An Intermediate in the Reduction Pathway of Ferric Salts with MeMgBr. *J. Am. Chem. Soc.* **2014**, *136*, 15457; (k) Muñoz III, S. B.; Daifuku, S. L.; Brennessel, W. W.; Neidig, M. L. Isolation, Characterization, and Reactivity of $Fe_8Me_{12}^-$: Kochi's *S* = 1/2 Species in Iron-Catalyzed Cross-Couplings with MeMgBr and Ferric Salts. *J. Am. Chem. Soc.* **2016**, *138*, 7492; (l) Zhurkin, F. E.; Wodrich, M. D.; Hu, X. A Monometallic Iron(I) Organoferrate. *Organometallics*, **2017**, *36*, 499; (m) Muñoz III, S. B.; Daifuku, S. L.; Sears, J. D.; Baker, T. M.; Carpenter, S. H.; Brennessel, W. W.; Neidig, M. L. The N-Methylpyrrolidone (NMP) Effect in Iron-Catalyzed Cross-Coupling with Simple Ferric Salts and MeMgBr. *Angew. Chem. Int. Ed.* **2018**, *57*, 6496; (n) Parchomyk, T.; Demeshko, S.; Meyer, F.; Koszinowski, K. Oxidation States, Stability, and Reactivity of Organoferrate Complexes. *J. Am. Chem. Soc*. **2018**, *140*, 9709; (o) Weinberger, B.; Tanguy, G.; Des Abbayes, H. A mild phase transfer synthesis of the ylid adduct $(CO)_4FeCH_2P(C_6H_5)_3$ from iron pentacarbonyl and dichloromethane: Evidence for the transient generation of the tetracarbonyl ferrate anion $Fe(CO)_4^{2-}$. *J. Organomet. Chem.*, **1985**, *280*, C31; (p) Collman, J. P.; Finke, R. G.; Cawse, J. N.; Brauman, J. I. Oxidative-addition reactions of the disodium tetracarbonylferrate supernucleophile. *J. Am. Chem. Soc.* **1977**, *99*, 2515; (q) Collman, J. P. Disodium tetracarbonylferrate, a transition metal analog of a Grignard reagent. *Acc. Chem. Res*. **1975**, *8*, 342.

(4) (a) Albores, P.; Carella, L. M.; Clegg, W.; Garcia-Alvarez, P.; Kennedy, A. R.; Klett, J.; Mulvey, R. E.; Rentschler, E.; Russo, L. Direct C-H Metalation with Chromium(II) and Iron(II): Transition-Metal Host / Benzenediide Guest Magnetic Inverse-Crown Complexes. *Angew. Chem. Int. Ed*. **2009**, *48*, 3317; (b) Maddock, L. C. H.; Nixon, T.; Kennedy, A. R.; Probert, M. R.; Clegg, W.; Hevia, E. Utilising Sodium-Mediated Ferration for Regioselective Functionalisation of Fluoroarenes via C−H and C−F Bond Activations. *Angew. Chem. Int. Ed.*, **2018**, *57*, 187; (c) Nagaradja, E.; Chevallier, F.; Roisnel, T.; Jouikov, V.; Mongin, F. Deprotonative metalation of aromatic compounds using mixed lithium–iron combinations. *Tetrahedron* **2012**, *68*, 3063; (d) Wunderlich, S. H.; Knochel, P. Preparation of Functionalized Aryl Iron(II) Compounds and a Nickel-Catalyzed Cross-Coupling with Alkyl Halides. *Angew. Chem. Int. Ed*. **2009**, *48*, 9717.

(5) (a) Strohmeier, W.; Müller, F. -J. Notiz zur photochemischen Herstellung von Eisenpentacarbonyl-Derivaten *Chem. Ber*. **1969**, *102*, 3613; (b) Bigorgne, M. Étude spectroscopique Raman et infrarouge de $Fe(CO)_5$, $Fe(CO)_4L$ et trans-$Fe(CO)_3L_2$ (L = PMe_3, $AsMe_3$, $SbMe_3$) I. Attribution des bandes de $Fe(CO)_5$. *J. Organomet. Chem*. **1970**, *24*, 211.

(6) Tinnermann, H.; Fraser, C.; Young, R. D. Zero valent iron complexes as base partners in frustrated Lewis pair chemistry. *Dalton Trans.* **2020**, *49*, 15184.

(7) (a) Braunschweig, H.; Dewhurst, R. D.; Hupp, F.; Schneider, C. Silver(i) and thallium(i) cations as unsupported bridges between two metal bases. *Chem. Commun.* **2014**, *50*, 15685; (b) Braunschweig, H.; Dewhurst, R. D.; Hupp, F.; Kaufmann, C.; Phukan, A. K.; Schneider, C.; Ye, Q. Gauging metal Lewis basicity of zerovalent iron complexes via metal-only Lewis pairs. *Chem. Sci*. **2014**, *5*, 4099; (c) Demerseman, B.; Bouquet, G.; Bigorgne, M. Basicité des complexes trans-$L_2(CO)_3Fe$ liaisons fer-mercure dans les complexes $L_2(CO)_3Fe{\rightarrow}HgX_2{\leftrightarrow}[L_2(CO)_3Fe\text{-}HgX]^+X^-$. *J. Organomet. Chem.* **1972**, *35*, 341.

(8) For examples of alkali metal adducts of $[FeL_n(CO)]^{m-}$, see: (a) Sciarone, T. J. J.; Nijhuis, C. A.; Meetsma, A.; Hessen, B. Synthesis and reactivity of mono(amidinate) organoiron(ii) complexes. *Dalton Trans*., **2006**, 4896; (b) Loewen, N. D.; Berben, L. A. Secondary Coordination Sphere Design to Modify Transport of Protons and CO_2. *Inorg. Chem.*, **2019**, *58*, 16849; (c) Wright, R. J.; Zhang, W.; Yang, X.; Fasulo, M.; Tilley, T. D. Isolation, observation, and computational modeling of proposed intermediates in catalytic proton reductions with the hydrogenase mimic $Fe_2(CO)_6S_2C_6H_4$. *Dalton Trans*., **2012**, *41*, 73; (d) Saouma, C. T.; Lu, C. C.; Day, M. W.; Peters, J. C. CO_2 reduction by Fe(i): solvent control of C–O cleavage versus C–C coupling. *Chem. Sci.*, **2013**, *4*, 4042; (e) Joseph, C.; Kuppuswamy, S.; Lynch, V. M.; Rose, M. J. Fe_5Mo Cluster with Iron-Carbide and Molybdenum-Carbide Bonding Motifs: Structure and Selective Alkyne Reductions. *Inorg. Chem*. **2018**, *57*, 20; (f) Oberem, E.; Roesel, A. F.; Rosas-Hernández, A.; Kull, T.; Fischer, S.; Spannenberg, A.; Junge, H.; Beller, M.; Ludwig, R.; Roemelt, M.; Francke, R. Mechanistic Insights into the Electrochemical Reduction of CO_2 Catalyzed by Iron Cyclopentadienone Complexes. *Organometallics*, **2019**, *38*, 1236.

(9) Liu, Z.; Lee, J. H. Q.; Ganguly, R.; Vidovic, D. A Well-Defined Aluminum-Based Lewis Acid as an Effective Catalyst for Diels–Alder Transformations. *Chem. Eur. J*. **2015**, *21*, 11344.

(10) Shannon, R. D. Revised effective ionic radii and systematic studies of interatomic distances in halides and chalcogenides. *Acta Cryst*. **1976,** *A32*, 751.

(11) For examples of noble metal activation of DCM, see: (a) Marder, T. B.; Fultz, W. C.; Calabrese, J. C.; Harlow, R. L.; Milstein, D. Activation of dichloromethane by basic rhodium(I) and iridium(I) phosphine complexes. Synthesis and structures of fac-$[Rh(PMe_3)_3Cl_2(CH_2PMe_3)]Cl{\cdot}CH_2Cl_2$ and trans-

[Rh(Me$_2$PCH$_2$CH$_2$PMe$_2$)$_2$Cl(CH$_2$Cl)]Cl. *J. Chem. Soc., Chem. Commun.* **1987**, *0*, 1543; (b) Blank, B.; Glatz, G.; Kempe, R. Single and Double C-Cl-Activation of Methylene Chloride by P,N-ligand Coordinated Rhodium Complexes. *Chem. - An Asian J.* **2009**, *4*, 321; (c) Adams, G. M.; Chadwick, F. M.; Pike, S. D.; Weller, A. S. A CH_2Cl_2 complex of a [Rh(pincer)]$^+$ cation. *Dalton Trans.* **2015**, *44*, 6340; (d) Abo-Amer, A.; McCready, M. S.; Zhang, F.; Puddephatt, R. J. The role of solvent in organometallic chemistry — Oxidative addition with dichloromethane or chloroform. *Can. J. Chem*. **2012**, *90*, 46; (e) Huser, M.; Youinou, M. T.; Osborn, J. A. Chlorocarbon Activation: Catalytic Carbonylation of Dichloromethane and Chlorobenzene. *Angew. Chem. lnt. Ed.* **1989**, *28*, 1386.

(12) (a) Kandler, H.; Bidell, W.; Jänicke, M.; Knickmeier, M.; Veghini, D.; Berke, H. Functionalized Iron Ketene Complexes from Carbonyl Coupling Reactions. *Organometallics*, **1998**, *17*, 960; (b) Ghisolfi, A.; Condello, F.; Fliedel, C.; Rosa, V.; Braunstein, P. Facile and Room-Temperature Activation of C_{sp3}–Cl Bonds by Cheap and Air-Stable Nickel(II) Complexes of (N-Thioether) DPPA-Type Ligands. *Organometallics* **2015**, *34*, 2255; (c) Csok, Z.; Vechorkin, O.; Harkins, S. B.; Scopelliti, R.; Hu, X. Nickel Complexes of a Pincer NN_2 Ligand: Multiple Carbon−Chloride Activation of CH_2Cl_2 and $CHCl_3$ Leads to Selective Carbon−Carbon Bond Formation. *J. Am. Chem. Soc.* **2008**, *130*, 8156.

(13) Pańkowski, M.; Bigorgne, M. Syntheses et isomerisation de complexes de la serie des derives halocarbonyle due fer: $[FeX(CO)_{5-n}L_n]^+$, $FeX_2(CO)_{4-n}L_n$ et $[FeX_3(CO)_3]^-$ (L = PMe$_3$; n = 1, 2, 3; X = Cl, Br, I). *J. Organomet. Chem.*, **1977**, *125*, 231.

(14) For examples of iron mediated Wurtz couplings, see: (a) Khurana, J. M.; Sushma, C.; Maikap, G. C. Facile reductive coupling of benzylic halides with ferrous oxalate dihydrate. *Org. Biomol. Chem.*, **2003**, *1*, 1737; (b) Nakanishi, S.; Oda, T.; Ueda, T.; Otsuji, Y. Reaction of benzylic and allylic halides with iron-carbonyl clusters. *Chem. Lett.*, **1978**, *7*, 1309; (c) Buu-Hoi, N. P.; Hoan, N. The reaction of α-halogenated arylalkanes with metal powders in hydroxylated media. *J. Org. Chem.*, **1949**, *14*, 1023; (d) Onuma, K.; Yamashita, J.; Hashimoto, H. The reductive coupling reactions of some chloromethylbenzene derivatives with iron(II) complexes. II. Reduction by anhydrous iron(II) chloride and lithium chloroferrate(II). *Bull. Chem. Soc. Jpn*., **1973**, *46*, 333.

(15) For examples of catalytic hydrodehalogenation of aliphatic halides, see: (a) Haibach, M. C.; Stoltz, B. M.; Grubbs, R. H. Catalytic Reduction of Alkyl and Aryl Bromides Using Propan-2-ol. *Angew. Chem. Int. Ed.* **2017**, *56*, 15123; (b) Narayanam, J. M. R.; Tucker, J. W.; Stephenson, C. R. J. Electron-Transfer Photoredox Catalysis: Development of a Tin-Free Reductive Dehalogenation Reaction. *J. Am. Chem. Soc*. **2009**, *131*, 8756; (c) Alonso, F.; Beletskaya, I. P.; Yus, M. Metal-Mediated Reductive Hydrodehalogenation of Organic Halides. *Chem. Rev.* **2002**, *102*, 4009.

(16) (a) Cabrera-Trujillo, J. J.; Fernandez, I. Understanding the C–F Bond Activation Mediated by Frustrated Lewis Pairs: Crucial Role of Noncovalent Interactions. *Chem. Eur. J.*, **2020**, 10.1002/chem.202004733; (b) Mandal, D.; Gupta, R.; Young, R. D. Selective Monodefluorination and Wittig Functionalization of gem-Difluoromethyl Groups to Generate Monofluoroalkenes. *J. Am. Chem. Soc*. **2018**, *140*, 10682; (c) Mandal, D.; Gupta, R.; Jaiswal, A. K.; Young, R. D. Frustrated Lewis-Pair-Meditated Selective Single Fluoride Substitution in Trifluoromethyl Groups. *J. Am. Chem. Soc*. **2020**, *142*, 2572; (d) Gupta, R.; Jaiswal, A. K.; Mandal, D.; Young, R. D. A Frustrated Lewis Pair Solution to a Frustrating Problem: Mono-Selective Functionalization of C–F Bonds in Di- and Trifluoromethyl Groups. *Synlett*, **2020**, *31*, 933.

(17) Hedström, A.; Izakian, Z.; Vreto, I.; Wallentin, C. -J.; Norrby, P. -O. On the Radical Nature of Iron-Catalyzed Cross-Coupling Reactions. *Chem. Eur. J*. **2015**, *21*, 5946.

(18) For examples of 1,4-CHD being used as a radical scavenger, see: (a) Mutra, M. R.; Kudale, V. S.; Li, J.; Tsai, W. -H.; Wang, J. -J. Alkene versus alkyne reactivity in unactivated 1,6-enynes: regio- and chemoselective radical cyclization with chalcogens under metal- and oxidant-free conditions. *Green Chem.*, **2020**, *22*, 2288; (b) Gonza´lez, I.; Pla-Quintana, A.; Roglans, A.; Dachs, A.; Sola`, M.; Parella, T.; Farjas, J.; Roura, P.; Lloveras, V.; Vidal-Gancedo, J. Ene reactions between two alkynes? Doors open to thermally induced cycloisomerization of macrocyclic triynes and enediynes. *Chem. Commun.*, **2010**, *46*, 2944–2946.

(19) Xu, M.; Jupp, A. R.; Qu, Z. -W.; Stephan, D. W. Alkali Metal Species in the Reversible Activation of H_2. *Angew. Chem. Int. Ed*. **2018**, *57*, 11050.

(20) (a) Carmona, E.; Marin, J. M.; Paneque, M.; Poveda, M. L. New nickel o-methylbenzyl complexes. Crystal and molecular structures of Ni(η^3-CH$_2$C$_6$H$_4$-o-Me)Cl(PMe$_3$) and Ni$_3$(η^1-CH$_2$C$_6$H$_4$-o-Me)$_4$(PMe$_3$)$_2$(μ_3-OH)$_2$. *Organometallics* **1987**, *6*, 1757; (b) Zell, T.; Radius, U. Carbon Halide Bond Activation of Benzyl Chloride and Benzyl Bromide Using An NHC-Stabilized Nickel(0) Complex. *Z. Anorg. Allg. Chem.* **2011**, *637*, 1858; (c) Lu, Z.; Fu, G. C. Alkyl–Alkyl Suzuki Cross-Coupling of Unactivated Secondary Alkyl Chlorides. *Angew. Chem. Int. Ed.* **2010**, *49*, 6676; (d) Ateşin, T. A.; Li, T.; Lachaize, S.; Brennessel, W. W.; García, J. J.; Jones, W. D. Experimental and Theoretical Examination of C−CN and C−H Bond Activations of Acetonitrile Using Zerovalent Nickel. *J. Am. Chem. Soc*. **2007**, *129*, 7562; (e)

Table of Contents artwork